

# Location dependent flight cost differences from the lunar surface to an orbital fuel depot and its influence on ISRU location selection

Sven J. Steinert<sup>1,\*</sup>, Paul Zabel<sup>2</sup> and Dominik Quantius<sup>2</sup>

<sup>1</sup> School of Engineering and Design, Technical University of Munich (TUM), Munich, Germany

<sup>2</sup> Institute of Space Systems, Systemanalyse Raumsegment, German Aerospace Center (DLR), Bremen, Germany

Correspondence\*:

Sven Julius Steinert

sven.julius.steinert@outlook.com

## 2 ABSTRACT

With increasing relevance for lunar activities, the location selection for in situ resource utilization (ISRU) facilities is a necessary step to identify the most suitable configuration during mission planning. To raise information about the dominant location dependencies, a scenario was set up where an ISRU product is exported to an orbital depot and mass costs are used for classification. In the selected scenario, Oxygen is produced by an Ilmenite reduction plant and subsequently exported to the Lunar Gateway via an Oxygen-Hydrogen fueled launcher running in a round-trip, refueling Oxygen at the lunar surface and Hydrogen at the Lunar Gateway. It showed that the variations in transport costs can be either entirely avoided or have a recessive influence on the mission's total costs over an extended amount of time, such as 20 years. The identification of the top 10 most optimal locations for various resolutions were only slightly altered under consideration of flight costs compared to only considering the ISRU factors, which concludes the insignificance of flight cost dependencies for the analysed case.

**Keywords:** In situ resource utilization (ISRU), orbital fuel depot, delta v map, lunar outpost, location selection, Ilmenite reduction, Lunar Gateway, Near-rectilinear halo orbit (NRHO)

## 1 INTRODUCTION

The Moon and its currently unused resources are holding a great potential in economics and development for the human presence. The big collaborative field study of Kornuta et al. (2019) has shown, that an undertaking like this is technologically feasible which was presented in a commercial architecture. In contrast to Kornuta et al. (2019), where water ice in the permanently shadowed regions near the poles is focused as resource for Hydrogen and Oxygen via electrolysis, Oxygen could be also obtained through extraction from regolith. This involves downsides as Oxygen is only one propellant component and big machinery for regolith handling is required, but also opportunities as the abundance of Oxygen in regolith is truly vast with a combined weight percent up to 45% measured from Apollo return samples in Papike et al. (1982). This Oxygen is bonded to various elements which is where extraction methods as Hydrogen reduction of Ilmenite are focusing on one specific bond for an effective processing procedure. Therefore

27 propellant production does not need to be restricted to the polar regions, especially when a fully robotic In  
 28 situ resource utilization (ISRU) plant is feasible on the lunar surface and no life support systems and their  
 29 water resources are required. Optimization can be therefore based on the process factors to pick the most  
 30 optimal location globally. For this event, the goal of this analysis is to identify the leading significance of  
 31 two sections of process factors, the ISRU efficiency and the transport efficiency. In case of insignificance  
 32 by one of these influences, a prioritization is provided for future mission analysis on similar scenarios.

## 2 MATERIALS AND METHODS

33 The determination of influences is approached by an example scenario under which both ISRU hardware  
 34 costs and flight costs can be assigned and put together into a joined model under which comparisons can be  
 35 drawn, through mass costs as central unit. The example scenario consists out of an ISRU Oxygen plant on  
 36 the lunar surface and an orbital fuel depot where a comparable launcher is delivering and consuming the  
 37 produced Oxygen where the consumed Hydrogen is supplied externally.

### 38 2.1 ISRU Efficiency

39 When the optimal location is chosen by the highest ISRU efficiency, the whole production line has to be  
 40 inspected for location dependent factors first. Such location dependent factors are for example: raw material  
 41 concentration, solar irradiance, temperatures, flat surface conditions and further scenic requirements.  
 42 Hereby, the production method is decisive about the sensitivity to location depended factors. One prominent  
 43 extraction method is the Hydrogen reduction of Ilmenite which has been already demonstrated as in  
 44 Sargeant et al. (2020). In this process, the chemical bond of  $FeTiO_3$  is broken down by Hydrogen resulting  
 45 in the chemical Equation 1. The resulting water is electrolyzed where the Hydrogen is fed back and the net  
 46 reaction leaves pure Oxygen.



47 Hydrogen reduction of Ilmenite is chosen as the production method to be analyzed, which we expect to  
 48 feature a high dependency on the raw material concentration and therefore a strong location dependency  
 49 due to inhomogeneity of Ilmenite distribution. An alternative extraction method would be molten regolith  
 50 electrolysis which is mostly invariant over the lunar surface, which is why all results that are derived here  
 51 are therefore only applicable to the chosen production method.

#### 52 2.1.1 Model

53 To reduce model complexity, our model does include only the raw material concentration factor as  
 54 argument, the Ilmenite weight ratio  $w_{ilmenite}$ . While this does not cover all influences, the raw material  
 55 concentration covers a major part for the location dependency and does therefore serve as approximation  
 56 to a full location dependent model of Hydrogen reduction of Ilmenite. The hardware mass that has to be  
 57 moved to the lunar surface for ISRU operation serves as the criteria to be minimized. In a previous work of  
 58 (Guerrero-Gonzalez and Zabel, 2023) this hardware mass  $m_{hardware}$  depending on Ilmenite concentration  
 59 was determined for a combined production plant of Low Carbon Steel and Oxygen production. This  
 60 production plant was sized for an annually output of 23.9 t Oxygen and 25 t Low Carbon Steel. The model  
 61 consists out of a sum of required subsystems as defined in Equation 2 (Guerrero-Gonzalez and Zabel,  
 62 2023). These subsystems resemble all processing steps of required infrastructure to extract metal but also  
 63 Oxygen from lunar regolith. The stated power law equations are the fitted result of a sensitivity analysis, so

64 that the size of a given subsystem can be estimated explicitly dependent on the input parameter  $w_{\text{ilmenite}}$ ,  
 65 the Ilmenite concentration in weight percent (wt%).

$$\begin{aligned}
 y_0(x) &= 4036 \cdot x^{-1.064} - 9.59 && \text{Excavation} \\
 y_1(x) &= 17580 \cdot x^{-1.003} - 390.8 && \text{Handling} \\
 y_2(x) &= 19240 \cdot x^{-1.003} - 421.9 && \text{Beneficiation} \\
 y_3(x) &= 21780 \cdot x^{-1.198} + 120.3 && \text{O2 Extraction} \\
 y_4(x) &= 17910 \cdot x^{-1.265} + 1370 && \text{O2 Purification} \\
 y_5(x) &= 29650 \cdot x^{-0.7005} - 602.5 && \text{Metal Processing} \\
 y_6(x) &= 2541 \cdot x^{-0.7434} + 286.8 && \text{Gas Liquefaction \& Storage} \\
 y_7(x) &= 32440 \cdot x^{-0.8312} + 125.2 && \text{Thermal Control} \\
 y_8(x) &= 12000 \cdot x^{-0.9657} + 63.99 && \text{Power}
 \end{aligned}$$

66

$$m_{\text{hardware}}(x = w_{\text{ilmenite}} [\text{wt}\%]) = \sum_{i=0}^8 y_i(x) [\text{kg}] \quad (2)$$

67 Where in our scenario, only the Oxygen production is relevant, the additional subsystems as metal  
 68 processing scale in a similar way as the rest of the system so that the spread between low and high values  
 69 of  $w_{\text{ilmenite}}$  is not distorted significantly (88.69% spread to the maximum value vs. 89.97% spread without  
 70 metal processing, for  $1 \text{ wt}\% \leq w_{\text{ilmenite}} \leq 11 \text{ wt}\%$ ). Furthermore, this combined production plant could  
 71 still be a viable choice out of the synergistic effects of shared infrastructure. This is why we are choosing  
 72 this model to be our reference production plant as a whole rather than trimming subsystems. Therefore our  
 73 model is expressed in Equation 2 as well.

#### 74 2.1.2 Data Processing

75 To determine the cost for every location on the Moon, a global lunar map of Ilmenite weight ratio is  
 76 required. In a previous work by Hiroyuki Sato (Sato et al., 2017) an almost global TiO<sub>2</sub> abundance map  
 77 was created, where the values of weight percent (wt%) for TiO<sub>2</sub> are used as equivalent for Ilmenite. The  
 78 resulting map had a mask applied to leave only lunar Mare regions and had a limited latitude coverage  
 79 from  $-70^\circ$  to  $70^\circ$ . The limited coverage originates from the orbiter sensor data and its limitations in  
 80 measurement at an increasingly steep sunlight angle towards the poles. The initial data was created by the  
 81 Lunar Reconnaissance Orbiter Camera (LROC) Wide Angle Camera (WAC) which is our starting point to  
 82 recreate a similar dataset as (Sato et al., 2017) but on a global basis. The original WAC data segments are  
 83 joined together in Figure 1.

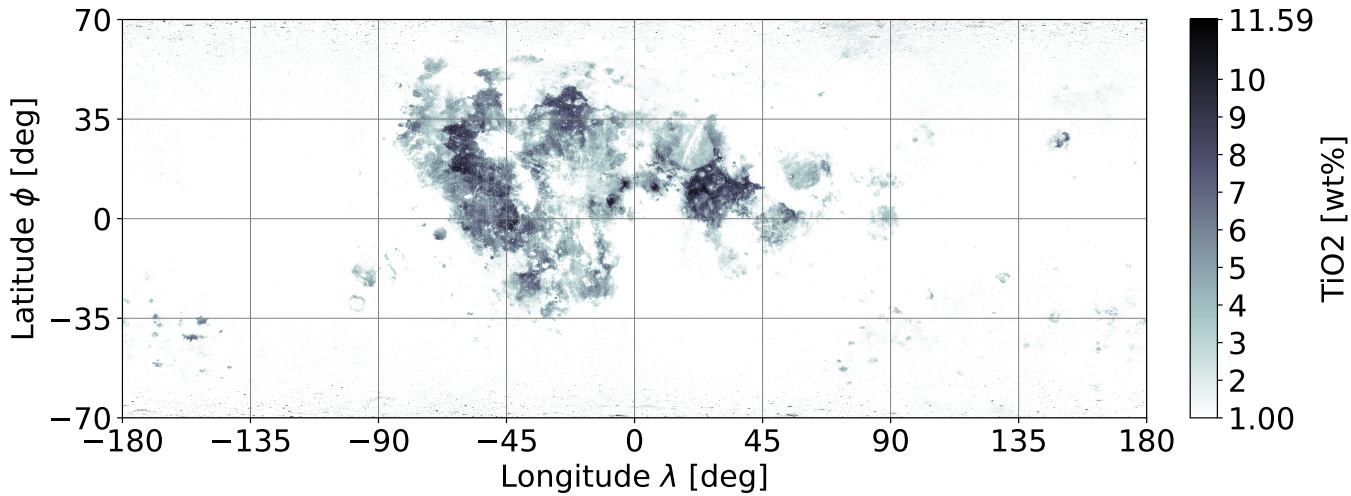


**Figure 1.** Combined original TiO<sub>2</sub> data of the WAC (Sato et al., 2017)

#### 84 2.1.2.1 Cleanup and Estimation

85 One problem is unusual high measurements towards the poles that are considered increasing noise which  
 86 is scattered through the entire longitudinal axis. The second problem is the incomplete coverage of latitude  
 87 and therefore the poles itself. To derive an estimation over the missing information at latitudinal coverage,  
 88 the following strategy is applied. If Ilmenite abundance correlates with the classification of Highlands /  
 89 Mare and the pole regions geology is featuring highland characteristics then the expected value of the  
 90 known highland region serves as an estimate of Ilmenite content at the poles.

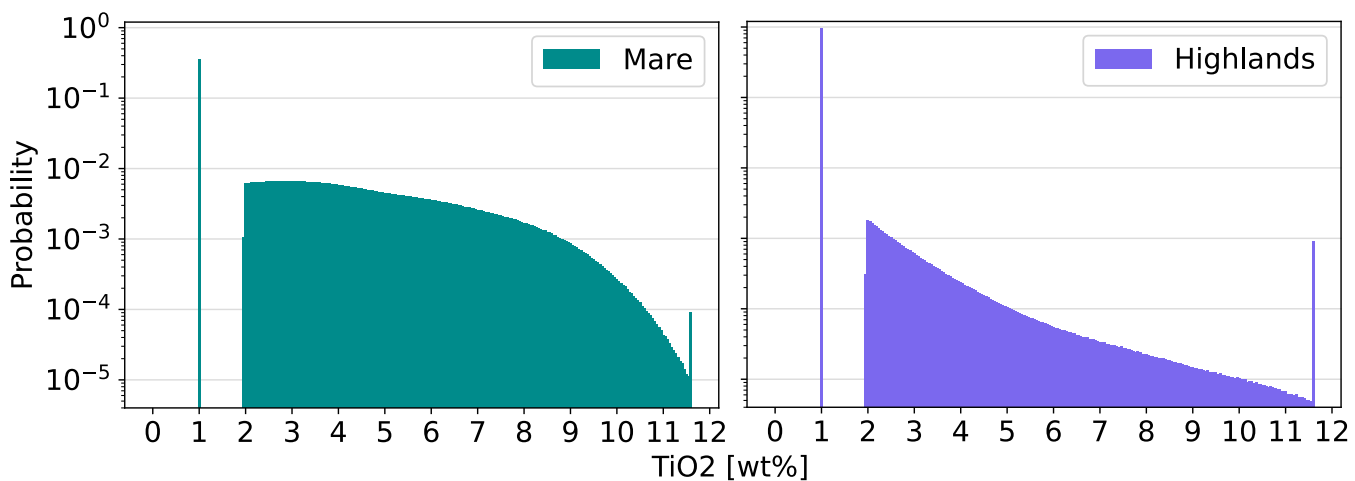


**Figure 2.** Distribution of Ilmenite content clustered into Highlands and Mare (equirectangular corrected) on combined WAC data with Mare boundaries from (Nelson et al., 2014)

91 As Figure 2 shows, the distribution characteristics of these two regions deviate considerably, whereby  
 92 the average abundance also differs from 3.38 wt% in Mare to 1.1 wt% in Highland regions. Therefore  
 93 the Ilmenite content correlation is given and the estimate over the missing latitudinal area of Highlands  
 94 is set to 1 wt% which also matches the WAC original assumption for values under the detection ratio.  
 95 To additionally remove the increasing noise at further extreme latitudes, a mask is created out of Mare

96 boundaries from (Nelson et al., 2014) merged with a constant separation at  $\phi = \pm 56^\circ$ . The replacement  
 97 values for the mask are equally set to 1 wt%. With both estimates applied, a low noise global Ilmenite map  
 98 is accomplished which can be seen in Figure 3.

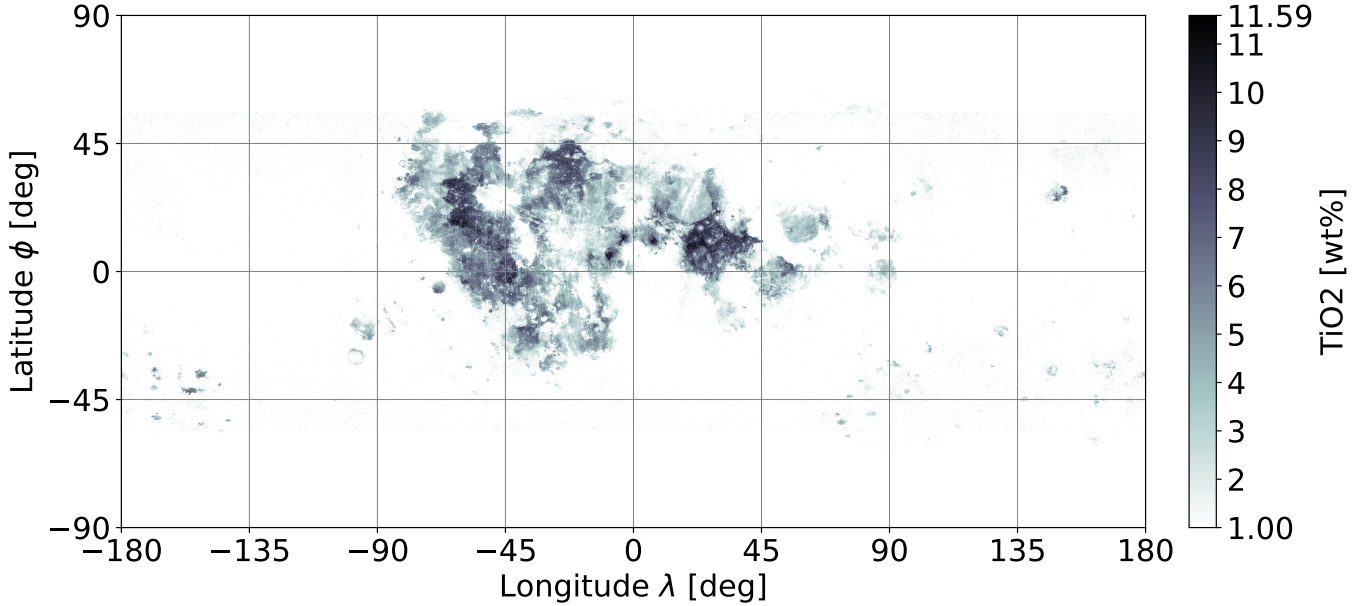


**Figure 3.** Global lunar Ilmenite map in weight percent through  $\text{TiO}_2$ , based on WAC data and estimates

### 99 2.1.2.2 ISRU Mass Cost Map

100 This global Ilmenite abundance map from Figure 3 is now used as input to Equation 2, which is resulting  
 101 in the location dependent ISRU hardware mass displayed in Figure 4.

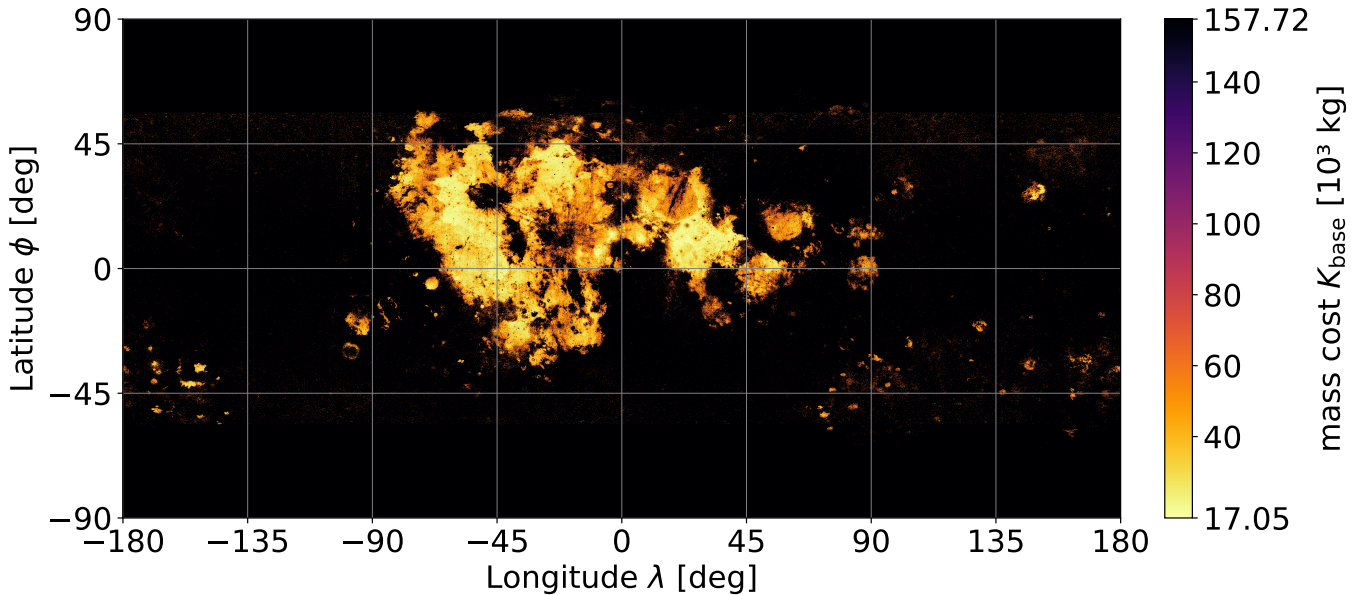


**Figure 4.** Location dependent ISRU hardware mass cost  $K_{\text{base}}$  in its base configuration of 23.9 t Oxygen per year

102 **2.2 Transport efficiency**103 **2.2.1 Mission Planning**

104 The mission is designed to be carried out by a single stage launcher to loop between the lunar surface  
 105 and the target orbit destination. The Oxygen fuel component and the Oxygen payload are refilled on lunar  
 106 ground at the ISRU production plant. The Hydrogen fuel component on the other hand is refilled at the fuel  
 107 depot where also the Oxygen payload is delivered. This Hydrogen is supplied from a different process,  
 108 where Earth is the assumed origin for the associated equivalent mass costs later on. This results effectively  
 109 in an exchange of delivered Oxygen to deducted Hydrogen from the station. A multi staged launcher or a  
 110 shuttle exchange system was neglected for this analysis but would hold the potential to further increase the  
 111 transport efficiency.

112 **2.2.2 Orbital Fuel Depot Location**

113 The primary requirement of the fuel depot location is its accessibility from both the supplying and  
 114 consuming units. For an interplanetary or cis-lunar logistic hub near Earth, Liberation points are especially  
 115 suited as considered by previous studies from Perrin and Casler (2016). Similar to Liberation points, their  
 116 corresponding halo orbits are offering the benefits of accessibility as well. In the case for an interplanetary  
 117 logistic hub near Earth which is supplied by the lunar surface, the currently planned Lunar Gateway on its  
 118 Near-rectilinear halo orbit (NRHO) fits prodigiously as a theoretical test bed for this purpose. Additionally,  
 119 an NRHO fuel depot was also considered in the commercial lunar propellant export study by Kornuta  
 120 et al. (2019). Which is why the Lunar Gateway orbit is chosen to be analysed in this scenario as the export  
 121 destination and considered a fuel depot.

122 **2.2.3 Target Orbit**

123 For the selected fuel depot location at the Lunar Gateway, the target orbit is a specific NRHO that is in a  
 124 9:2 Lunar Synodic Resonance with an average perilune of  $h_{peri} = 3557 \text{ km}$  and an average orbital period  
 125 of  $T = 6.562 \text{ days}$  (Lee, 2019). It is worth mentioning that this orbit has a varying polar crossing as well  
 126 as other time dependent changes in its trajectory which are often simplified to more static conditions for  
 127 analysis (Whitley et al., 2018).

128 **2.2.4 Delta-v Estimation**

129 First of all, regardless of the mission or the trajectory, planetary conditions such as ground elevation and  
 130 surface velocity are influencing the required  $\Delta v$ . These influences are now briefly assessed for the Moon to  
 131 determine their relevance.

132 **2.2.4.1 Celestial Influences**

133 The initial radial distance to the Moon's center of mass  $r(\phi, \lambda)$  influences the ideal  $\Delta v$  demand directly  
 134 as shown for an ascent into a circular orbit at  $r_{orbit}$  with standard gravity  $g_0$  and standard gravitational  
 135 parameter  $\mu$  in Equation 3.

$$\Delta v_{ideal}(\phi, \lambda) = \sqrt{v_{orbit}^2 + v_{ascent}^2} = \sqrt{\left(\frac{\mu}{r_{orbit}}\right) + \left(2 \cdot g_0 \cdot \left[r(\phi, \lambda) - \frac{r(\phi, \lambda)^2}{r_{orbit}}\right]\right)} \quad (3)$$

136 Global ground elevation data is now used in the form of a displacement map (Ernie Wright and Noah  
 137 Petro, 2019), which originates on Lunar Orbiter Laser Altimeter (LOLA) measurements (David E. Smith,

138 2015). The elevation ranges from -9.115 km to 10.757 km with regard to the reference radius  $r_{\text{ref}}$  of 1737.4  
 139 km and therefore defines  $r(\phi, \lambda)$  globally. The displacement map is shown in Figure 5.

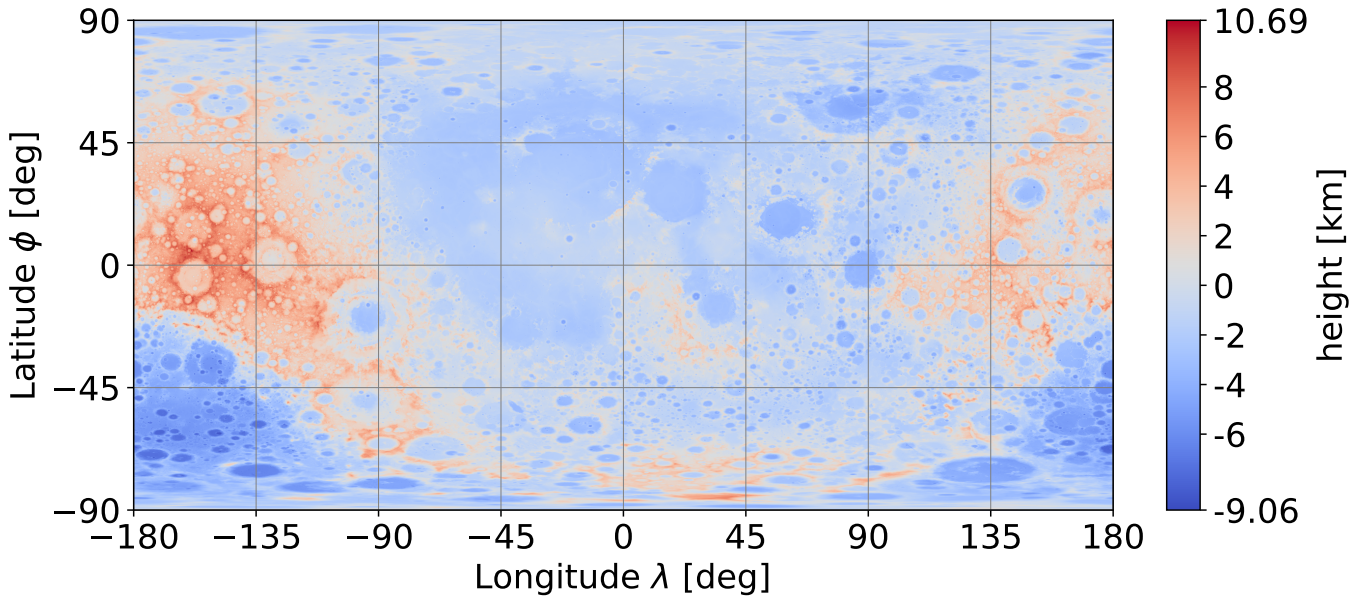


**Figure 5.** Lunar displacement map to reference radius ( $r_{\text{ref}} = 1737.4 \text{ km}$ ). Data from NASA CGI Kit (Ernie Wright and Noah Petro, 2019) based on (David E. Smith, 2015)

Evaluating the extreme values on a Low Lunar Orbit (LLO) at 100 km altitude ( $r_{\text{orbit}} = 1837.4 \text{ km}$ ) with Equation 3 yields:

$$\begin{aligned}\Delta v_{\min} &= \Delta v_{\text{ideal}}(\max \{r(\phi, \lambda)\}) = 1725.187 \frac{\text{m}}{\text{s}} \\ \Delta v_{\max} &= \Delta v_{\text{ideal}}(\min \{r(\phi, \lambda)\}) = 1725.204 \frac{\text{m}}{\text{s}}\end{aligned}$$

140 The influence on  $\Delta v$  from ground elevation is therefore at the order of 0.001 % which is extremely low.  
 141 The second celestial influence, the initial surface velocity  $v_0$  is either an additional  $\Delta v$  demand or a  $\Delta v$   
 142 reduction, depending on the shared velocity components to the launch direction. Together with the sidereal  
 143 rotation period and the assumption of a spherical lunar surface of  $r_{\text{ref}}$ , the surface velocity can be given as  
 144 a function of Latitude  $\phi$  as displayed in Equation 4.

$$v_0(\phi) = \frac{2\pi}{27.322 \text{ days}} \cdot \cos(\phi) \cdot r_{\text{ref}} \quad (4)$$

145 Evaluating the extreme points of polar and equatorial locations on Equation 4 yields:

$$\begin{aligned}\Delta v_{\min} &= \Delta v_0(\phi = \pm 90^\circ) = 0.000 \frac{\text{m}}{\text{s}} \\ \Delta v_{\max} &= \Delta v_0(\phi = 0^\circ) = \pm 4.624 \frac{\text{m}}{\text{s}}\end{aligned}$$

146 Comparing this range  $|\Delta v_{\max}| - \Delta v_{\min}$  to the ascent from the reference radius to a circular 100 km  
 147 LLO being  $\Delta v_{\text{ideal}}(r_{\text{ref}}) = 1725.196 \frac{\text{m}}{\text{s}}$  gives the  $\Delta v$  influence of the surface velocity to be at the order  
 148 of 0.27 % which is significantly more than the elevation influences but still considerably low.

149 **2.2.4.2 Transfer Options**

150 Explicit Transfers from any lunar geodetic point to NRHOs and vice versa are a high-fidelity problem  
 151 which is usually solved non-analytically as in (Trofimov et al., 2020). Additionally, there are multiple  
 152 transfer strategies that can be deployed for different optimisation goals. Between optimisation of required  
 153  $\Delta v$  and transfer time, two transfer options are being analysed for our chosen scenario.

154 First, a long duration transfer that features a very low required  $\Delta v$  of only  $664.9 \frac{m}{s}$  to a LLO at 100  
 155 km altitude, which is very close to the theoretical limit of  $654.8 \frac{m}{s}$  as minimum energy change (Whitley  
 156 et al., 2018). Also, it features an almost complete independency to surface location, which is reached  
 157 by something similar to a Three-Impulse transfer, where the lunar sphere of influence is left to circle  
 158 once around Earth before inserting again. This allows any inclination restrictions to vanish, but at a cost  
 159 of a 100.1 day long transfer time. If this transfer option is chosen, the influence of transfer efficiency  
 160 is extremely low and marginal to the ISRU dependencies derived in Chapter 2.1. In this case transfer  
 161 dependencies can be neglected and the location selection can be simplified to only ISRU efficiency.

162 Often however a 100 day transfer time is simply too long for certain applications, as it for example  
 163 induces general system lag time and therefore poor dynamics in propellant delivery adjustments in the case  
 164 of the subjected mission. For this reason, a second transfer option is analysed which is a direct transfer  
 165 trajectory between the NRHO and the surface from Trofimov et al. (2020), which features the shortest  
 166 transfer time of only hours but at the cost of higher  $\Delta v$  and location dependency. The direct transfer,  
 167 illustrated in Figure 6, is the subject of the following analysis in the following sub-chapters and serves as a  
 168 worst case scenario for an NRHO transfer in terms of location dependencies.

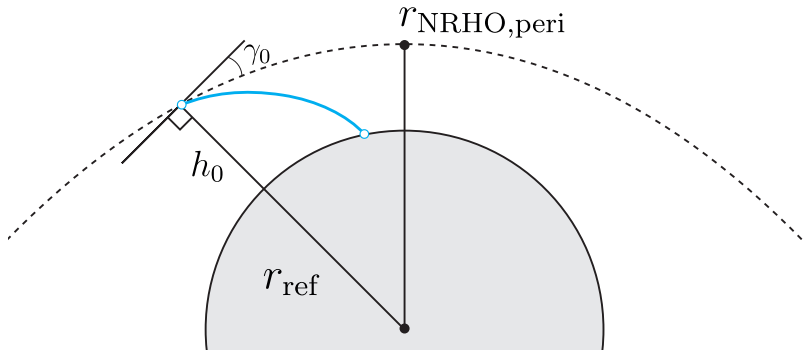


**Figure 6.** Direct decent trajectory scheme according to Trofimov et al. (2020)

169 **2.2.4.3 Data Processing**

170 In the previous work by Trofimov et al. (2020), a set of possible direct decent trajectories and their  
 171 associated landing point and  $\Delta v$  demand were identified. The resulting map of scatter points for the  
 172 southern 9:2 NRHO was taken as starting point to derive a global  $\Delta v$  map. As this result does not hold  
 173 the solutions of the cheapest trajectory for each location but rather all found solutions for a direct decent,  
 174 the data points can hold low and high cost solutions for the same location. Since for our mission planning  
 175 always the cheapest option for one location would be chosen, a minimum estimation is performed. This  
 176 estimation is done by splitting the map into 20 deg square tiles where constancy is assumed and the lowest  
 177 value is set for the whole tile. This tiling on an equirectangular projected map gives a higher resolution  
 178 towards the poles which is causing the problem, that in the southern polar region the solution coverage is so

179 low that only high cost solutions are present in one tile even though their neighbor tile features a low cost  
 180 solution. To mitigate this, the data has been cut from particular high costs trajectories of  $\Delta v > 2985.65 \frac{m}{s}$   
 181 which leaves a few southern pole tiles non defined. If that cutting of data would not be performed, up  
 182 to  $3300 \frac{m}{s}$  transfer options would have been carried over into the final map which are clearly high cost  
 183 solutions and would not be considered in a real mission. This process is visualized in Figure 7.

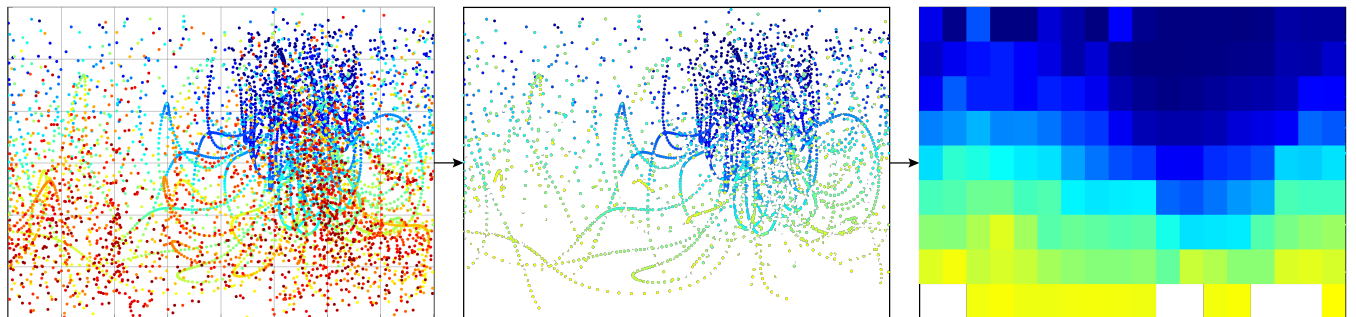


**Figure 7.** Processing of results from Trofimov et al. (2020) (left) to cutting of data (center) into minimum of 20 deg square tiles (right)

184 The non defined tiles are estimated through their longitudinal neighboring tiles via linear interpolation,  
 185 which was only necessary in tiles at the southern polar region where there is already a higher geodetic  
 186 resolution. This leads to our final  $\Delta v$  map, depicted in Figure 8.

#### 187 2.2.4.4 Delta v Map

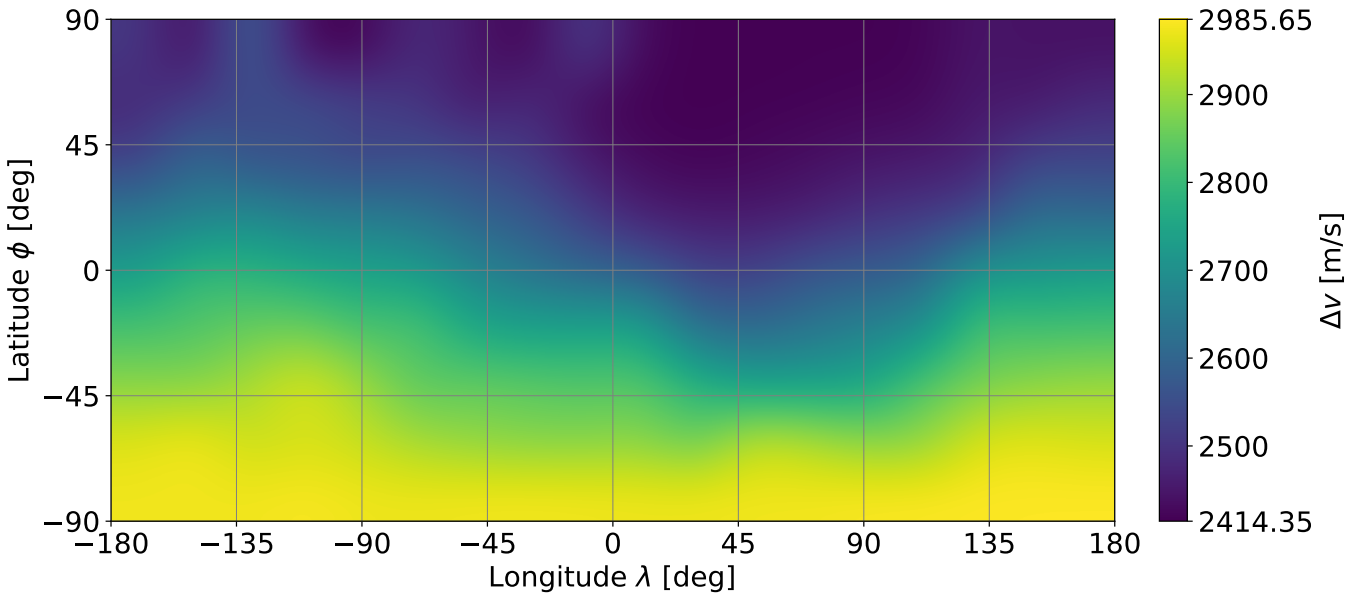


**Figure 8.** Required  $\Delta v$  for direct decent from southern 9:2 NRHO to the lunar surface (bicubic interpolated)

188 Even though this data of Figure 8 was computed for the decent only, it will serve as estimation for the  
 189 ascent as well, which is holding a bias as those problems are not entirely symmetric. Additionally, it should  
 190 be mentioned that even though a  $2414 \frac{m}{s}$  transfer is very viable, a transfer of around  $2900 \frac{m}{s}$  might be

rather replaced in a real world scenario by a different transfer strategy, as via a LLO with waiting time to save  $\Delta v$ . However in this analysis, Figure 8 defines  $\Delta v(\phi, \lambda)$  globally with  $\Delta v_{min} = 2414.35 \frac{m}{s}$  and  $\Delta v_{max} = 2985.65 \frac{m}{s}$ .

## 2.2.5 Transport Carrier

### 2.2.5.1 Reference Launcher

To derive associated transport mass costs, the previously determined  $\Delta v$  has to be applied on a specific launcher. The Argonaut, formerly known as the European Large Logistics Lander (EL3), is chosen as a starting point for this scenario. The initial configuration is based on the time of writing published information from the European Space Agency (2023) of 10 000 kg wet mass, 1600 kg dry mass and 2100 kg payload. Additionally a Hydrogen (H<sub>2</sub>), Oxygen (O<sub>2</sub>) propulsion system with an oxidizer fuel ratio of 6 and 400 s of specific impulse is assumed. When this original configuration is applied on our mission with  $\Delta v_{max}$  the fuel is running out before the round-trip can be completed. Therefore the launcher configuration has to be altered for our scenario needs.

### 2.2.5.2 Launcher Up-scaling

An up-scaling is performed, where the dry mass is kept constant at 1600 kg but fuel is added until the mission can be completed. The minimal viable system features an empty H<sub>2</sub> tank at arrival at the Gateway and an empty O<sub>2</sub> tank at the lunar surface. The Iteration scheme of the up-scaling is visualized in Figure 9, which can converge a minimal viable launcher for any given payload. The iteration is entered with an undersized launcher starting from the moon with “initial H<sub>2</sub>” as amount of Hydrogen in the tank at the lunar surface, “wet mass” which together with a constant dry mass indirectly represents the amount of Oxygen in the tank on the lunar surface, and “refill H<sub>2</sub>” which is the amount of Hydrogen refueled when arrived at the Lunar Gateway. When the  $\Delta v$  is applied in the simulated roundtrip, the undersized launcher is running into one of the defined failure cases, which indicate a particular missing propellant at some point of the mission. “O<sub>2</sub> empty” and “H<sub>2</sub> empty” describe the depletion of the Oxygen or Hydrogen tank during flight, which results in an increase of the desired propellant for the next iteration, whereby “O<sub>2</sub> leftover” and “H<sub>2</sub> leftover” trigger the analogue opposite. “H<sub>2</sub> insufficient” is a less obvious failure case when the launcher returned to the lunar surface but does not have enough Hydrogen to perform the next run for the roundtrip, as it only can be refueled at the Lunar Gateway and not on ground. Due to the fact that the launcher we entered the iteration is undersized, the value of “refill H<sub>2</sub>” can be approached unidirectional while still reaching convergence with a small enough increment of propellant.

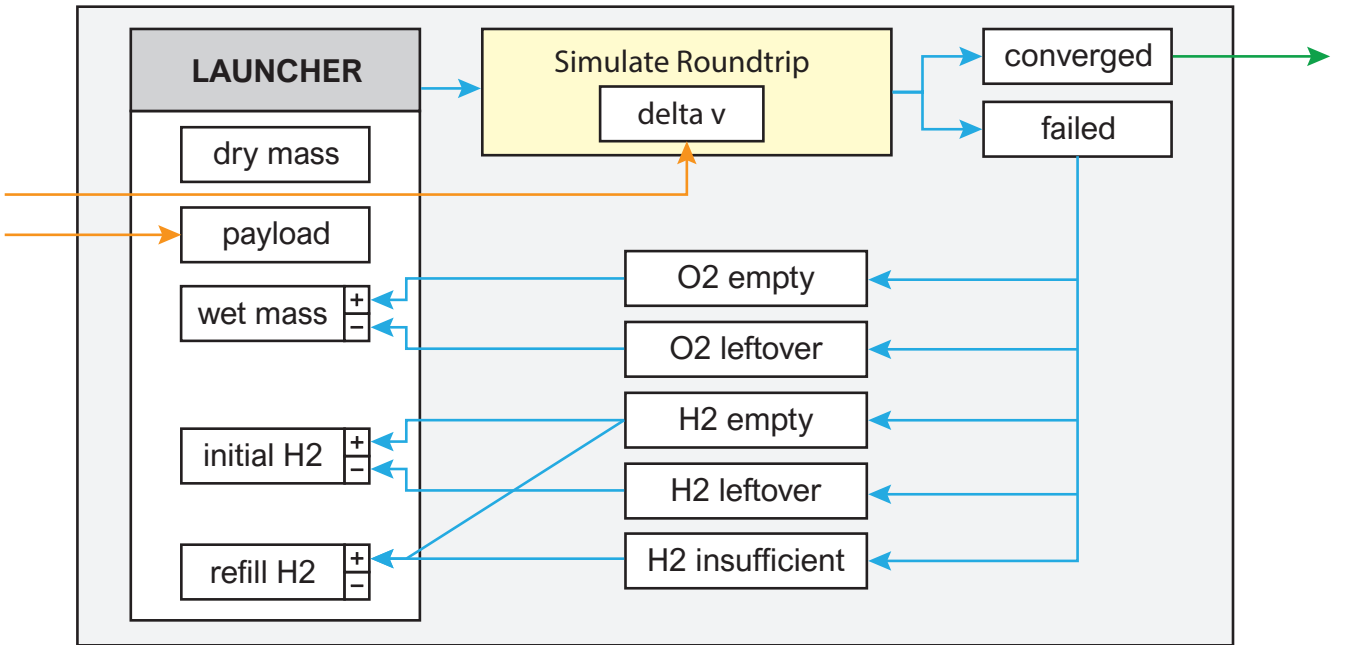


**Figure 9.** Launcher iteration scheme to converge a roundtrip for a given payload and  $\Delta v$

221 Since this method of up-scaling is effectively increasing the mass ratio ( $r_m = \frac{m_{\text{wet}}}{m_{\text{dry}}}$ ) of the launcher, this  
 222 assumption becomes increasingly unrealistic. Additionally, from the perspective of the fuel depot, Oxygen  
 223 is delivered but also Hydrogen is taken away, therefore effectively trading those masses by the exchange  
 224 ratio ( $r_{ex} = \frac{m_{\text{payload}}}{m_{\text{H2, refill}}}$ ). In order to bring a decision to what range of launchers shall be compared to derive  
 225 cost differences, Figure 10 visualises the parameter space between the exchange ratio  $r_{ex}$  and the mass  
 226 ratio of the launcher  $r_m$ .

227 Hereby there are two sections grayed out, once  $r_{ex} < 1$  out of economic reasonableness and second  
 228  $r_m > 10$  as a soft border of mass ratios for realistic single stage launchers. The selection of the chosen  
 229 launcher frames was done through a sequence of movements in the parameter space. Starting by the  
 230 economical reasonable exchange ratios of 1.5 and 2.0 (solid black lines, also called milestones), which  
 231 is then projected to their required mass ratio (dashed black line). This currently holds a set of constant  
 232 exchange ratio throughout the  $\Delta v$  range, in order to obtain comparable results however, the mass ratio  $r_m$   
 233 has to be constant over one set as it represents the efficiency of the launcher. Therefore, the maximum  
 234 value of the mass ratio (at  $\Delta v_{max}$ ) is set as constant over the  $\Delta v$  range which is then yielding the chosen  
 235 frame regarding the mass ratio (solid yellow line). When this set is then projected back onto the exchange  
 236 ratio (yellow dashed line), a span of exchange ratios is featured over the  $\Delta v$  range.

237 This concludes the two chosen frames (yellow lines) of:

$$r_m = 8.555 \quad \text{with } 1.5 \leq r_{ex} \leq 3.303$$

$$r_m = 10.688 \quad \text{with } 2.0 \leq r_{ex} \leq 3.889$$

238 To analyse the problem on two frames of different mass ratios is providing insight on the sensitivity  
 239 towards more efficient launchers in general and their influence on the location selection.

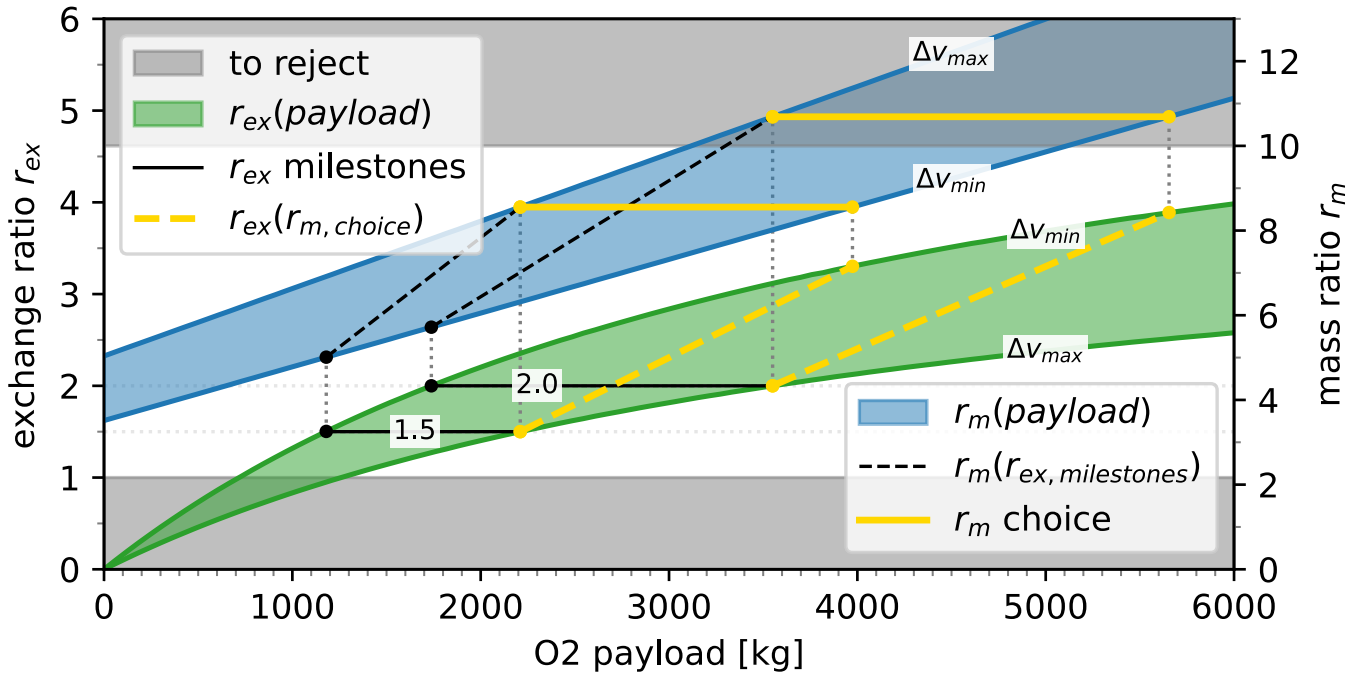


**Figure 10.** Exchange ratio  $r_{\text{ex}}$  and mass ratio  $r_m$  depending on payload size of the launcher over  $\Delta v$  range

#### 240 2.2.5.3 Spent Fuel

241 Through another iteration scheme, which is targeting the chosen mass ratio  $r_m$ , a launcher can be  
 242 converged for any  $\Delta v$ . The expended fuel is directly drawn from the simulated round-trip and normalized  
 243 by the payload size, which therefore can be combined into a direct mapping from required  $\Delta v$  to the spent  
 244 fuel  $k_{\text{Flight}}$  in kg per kg payload. This dependency can be seen in Figure 11 for both chosen mass ratios  
 245  $r_m = 8.6$  and  $r_m = 10.7$ . In this comparison, the higher mass ratio  $r_m = 10.7$  features a smaller absolute  
 246 and relative growth, which concludes that differences in spent fuel decrease in general by an increasing  
 247 launcher efficiency.

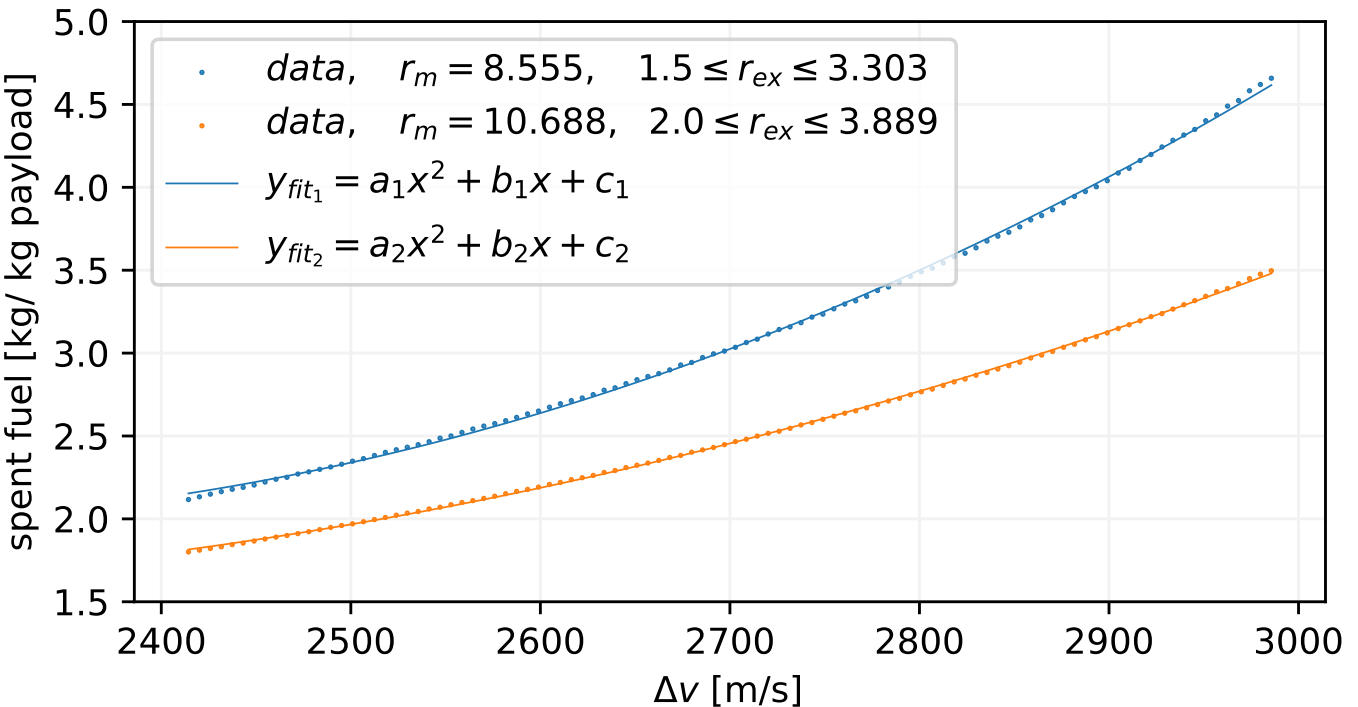


**Figure 11.** Relationship between required  $\Delta v$  and spent fuel  $k_{\text{Flight}}$  for both mass ratios

## 248 2.3 Joined Model

### 249 2.3.1 Total Cost Modelling

250 When both influences from Section 2.1 and Section 2.2 are combined, the comparable mass costs have to  
 251 be drawn from the mission scenario. Rather than assuming all expended fuel as transport cost, a separation  
 252 of the fuel components is done, due to the reason that the Oxygen is not being shipped from Earth but  
 253 rather fully supplied by the ISRU facility.

#### 254 2.3.1.1 Fix Costs

255 In order to meet the additional demand of Oxygen per year, that the launcher requires for transport,  
 256 the ISRU facility is scaled up linearly by its ISRU costs per kg Oxygen  $k_{\text{ISRU}}$  for each location and its  
 257 corresponding fuel requirements. The scaling factor originates from the base configuration costs from  
 258 Figure 4 and its annual base production  $m_{\text{base}} = 23.9 \text{ t}$ , which gives:  $k_{\text{ISRU}}(\phi, \lambda) = \frac{K_{\text{base}}(\phi, \lambda)}{m_{\text{base}}}$ . The  
 259 additional Oxygen demand per year is derived by the yearly payload  $m_{\text{pl,y}} = 8 \text{ t}$ , which has been set to  
 260 minimize scaling on the base configuration, the oxidiser-fuel-ratio  $r_{\text{of}}$  and the spent fuel  $k_{\text{Flight}}$  depending  
 261 on the two selected mass ratios  $r_m \in \{8.6, 10.7\}$ . Therefore the fix costs, which represent the Earth  
 262 supplied mass for the construction of the ISRU facility are:

$$27 K_{\text{Fix}}(\phi, \lambda, r_m) = K_{\text{base}}(\phi, \lambda) + k_{\text{ISRU}}(\phi, \lambda) \left( \left[ m_{\text{pl,y}} \cdot k_{\text{Flight}}(\phi, \lambda, r_m) \cdot \frac{r_{\text{of}}}{r_{\text{of}} + 1} \right] + m_{\text{year}} - m_{\text{base}} \right) \quad (5)$$

263 **2.3.1.2 Dynamic Costs**

264 The expended Hydrogen is considered fully as mass cost since it is taken from the Lunar Gateway depot  
 265 and assumed to be delivered by Earth. Hereby the cost level of the Lunar Gateway and the lunar surface  
 266 are simplified as equal from Earth to be comparable, which rather overestimates the Hydrogen's cost in  
 267 comparison to costs on the lunar surface when supplied from Earth. Therefore the dynamic costs, which  
 268 represent the Earth supplied mass for Hydrogen on the Lunar Gateway per year  $t$  are:

$$K_{\text{Dynamic}}(\phi, \lambda, t, r_m) = t \cdot m_{\text{pl,y}} \cdot k_{\text{Flight}}(\phi, \lambda, r_m) \cdot \frac{1}{r_{\text{of}} + 1} \quad (6)$$

269 **2.3.1.3 Total Costs**

270 Combining both  $K_{\text{Fix}}$  and  $K_{\text{Dynamic}}$ , the final total costs of the mission over location and time are:

$$K_{\text{Total}}(\phi, \lambda, t, r_m) = K_{\text{Fix}}(\phi, \lambda, r_m) + K_{\text{Dynamic}}(\phi, \lambda, t, r_m) \quad (7)$$

271 Applying Equation 7 with location dependent results from Section 2.1.2.2 and Section 2.2.5.3 gives the  
 272 total cost maps for the mission time of 20 years for  $r_m = 8.6$  in Figure 12 and  $r_m = 10.7$  in Figure 13.

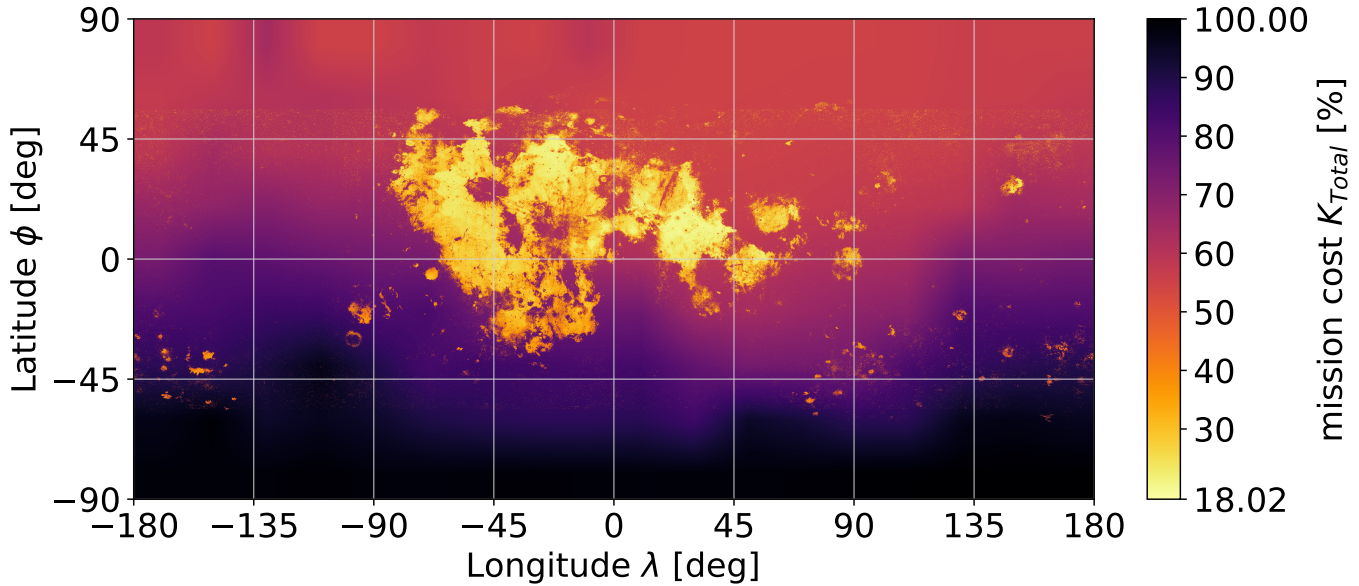


**Figure 12.** Location dependent total mission cost  $K_{\text{Total}}$  in % with  $t = 20$  years and  $r_m = 8.6$

273 In the direct comparison between Figure 12 and Figure 13, the flight cost influence is visibly less  
 274 pronounced for the increased mass ratio. Also, a reduced variation in total mission cost can be observed.

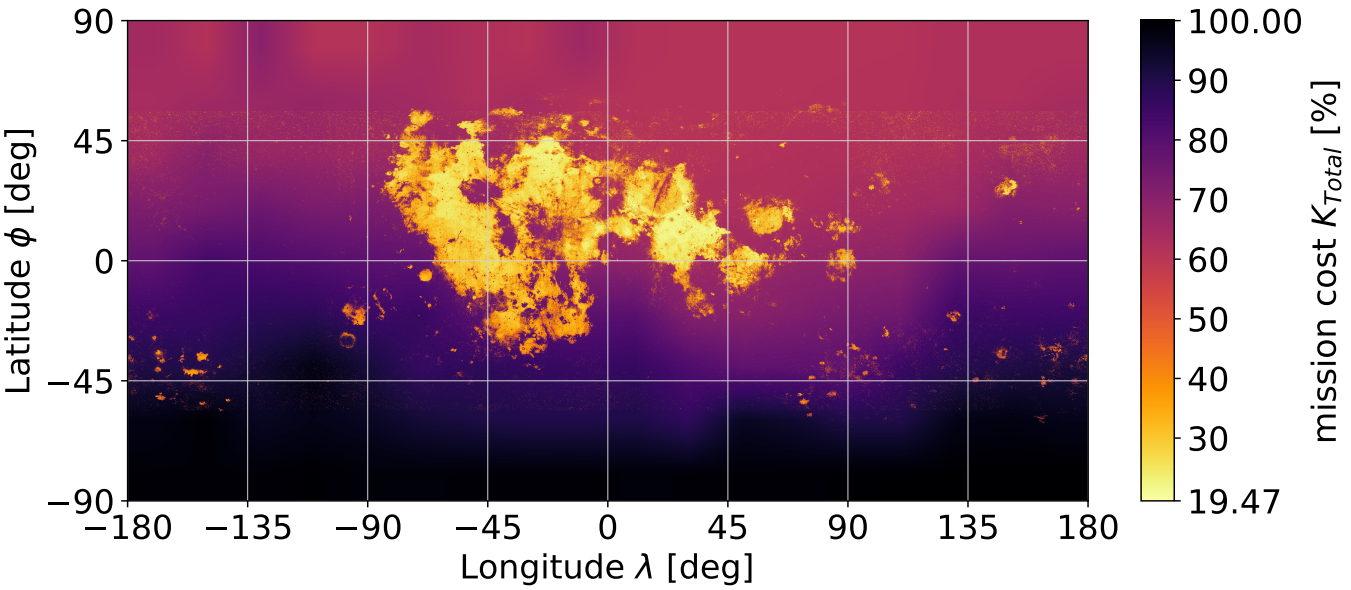


**Figure 13.** Location dependent total mission cost  $K_{\text{Total}}$  in % with  $t = 20$  years and  $r_m = 10.7$

### 3 RESULTS

#### 275 3.1 Flight Cost Influences

276 In the case of the availability of the long duration transfer (Section 2.2.4.2) which is able to diminish  
 277 location dependencies almost completely, as well as insignificant celestial influences (Section 2.2.4.1), the  
 278 effects on the missions location selection are eliminated by an assumable uniform  $\Delta v$  requirement.

279 Only under the short duration transfer strategy of a direct decent, location dependent  $\Delta v$  requirements  
 280 are prominent (Section 2.2.4.4) which translate to a significant difference in spent fuel (Section 2.2.5.3).  
 281 On the other side at the ISRU influence, Ilmenite reduction introduces vast location dependencies (Section  
 282 2.1.2.2), which overshadow the differences in the spent fuel, resulting in an ISRU feature dominated total  
 283 cost when both influences are combined (Section 2.3.1.3).

#### 284 3.2 Flight Cost Insignificance

285 To provide insight on the induced error when the flight costs are neglected completely, the best locations  
 286 from the ISRU model from Section 2.1 are compared to the best locations from the Joined model from  
 287 Section 2.3. In order to limit the possible locations, both models location dependent results are reduced  
 288 into geodetic square tiles of  $15^\circ$ ,  $5^\circ$  and  $1^\circ(\phi, \lambda)$ , to compare the behaviour on multiple resolutions. The  
 289 creation of the tiles  $T_{\phi \text{ index}, \lambda \text{ index}}$  was performed considering pixel area relation and yields an index  
 290 resolution of  $12 \times 24$ ,  $36 \times 72$  and  $180 \times 360$ . From the created tiles, the top 10 choices are ranked and  
 291 compared over the models. The top 10 choices make up the top 3.47 % for the  $15^\circ$  tiles, the top 0.39 %  
 292 for the  $5^\circ$  tiles and the top 0.015 % for the  $1^\circ$  tiles. In Table 1, the tiles are colorized by the ranking of  
 293 the ISRU model, from green as most optimal to orange as less optimal locations, giving the baseline for  
 294 comparison of ordering and featured tiles. Underneath the Joined model is shown in tree time steps, at 0,  
 295 10 and 20 years, providing a sense of temporal evolution of the featured tiles.

296 The induced error of the flight cost neglect increases over mission time, but nevertheless even at greater  
 297 time spans as 20 years, the top 10 of the Joined model are featuring many tiles which have been in the

	#1	#2	#3	#4	#5	#6	#7	#8	#9	#10
ISRU	$T_{5,8}$	$T_{5,13}$	$T_{3,10}$	$T_{4,7}$	$T_{6,9}$	$T_{3,8}$	$T_{5,14}$	$T_{4,13}$	$T_{6,8}$	$T_{4,10}$
J. t = 0	$T_{5,8}$	$T_{5,13}$	$T_{3,10}$	$T_{4,7}$	$T_{3,8}$	$T_{4,13}$	$T_{5,14}$	$T_{6,9}$	$T_{4,10}$	$T_{5,11}$
J. t = 10	$T_{5,13}$	$T_{3,10}$	$T_{5,8}$	$T_{4,13}$	$T_{4,7}$	$T_{3,8}$	$T_{5,14}$	$T_{6,9}$	$T_{4,10}$	$T_{5,11}$
J. t = 20	$T_{5,13}$	$T_{3,10}$	$T_{5,8}$	$T_{4,13}$	$T_{5,14}$	$T_{3,8}$	$T_{4,7}$	$T_{4,10}$	$T_{4,12}$	$T_{5,11}$
5° tiles	#1	#2	#3	#4	#5	#6	#7	#8	#9	#10
ISRU	$T_{15,40}$	$T_{14,24}$	$T_{16,41}$	$T_{14,23}$	$T_{16,40}$	$T_{12,23}$	$T_{10,31}$	$T_{13,24}$	$T_{15,25}$	$T_{15,42}$
J. t = 0	$T_{15,40}$	$T_{16,41}$	$T_{16,40}$	$T_{14,24}$	$T_{10,31}$	$T_{15,42}$	$T_{15,43}$	$T_{14,23}$	$T_{15,41}$	$T_{16,42}$
J. t = 10	$T_{15,40}$	$T_{16,41}$	$T_{16,40}$	$T_{15,42}$	$T_{10,31}$	$T_{15,43}$	$T_{15,41}$	$T_{16,42}$	$T_{17,40}$	$T_{11,31}$
J. t = 20	$T_{15,40}$	$T_{16,41}$	$T_{15,42}$	$T_{15,43}$	$T_{16,40}$	$T_{10,31}$	$T_{15,41}$	$T_{16,42}$	$T_{11,31}$	$T_{14,41}$
1° tiles	#1	#2	#3	#4	#5	#6	#7	#8	#9	#10
ISRU	$T_{79,204}$	$T_{81,201}$	$T_{80,200}$	$T_{72,118}$	$T_{80,201}$	$T_{84,171}$	$T_{72,117}$	$T_{81,199}$	$T_{72,116}$	$T_{80,204}$
J. t = 0	$T_{79,204}$	$T_{81,201}$	$T_{80,200}$	$T_{80,201}$	$T_{80,204}$	$T_{81,199}$	$T_{80,203}$	$T_{79,203}$	$T_{80,199}$	$T_{81,200}$
J. t = 10	$T_{79,204}$	$T_{80,200}$	$T_{80,201}$	$T_{81,201}$	$T_{80,204}$	$T_{79,203}$	$T_{80,203}$	$T_{76,201}$	$T_{78,218}$	$T_{78,204}$
J. t = 20	$T_{79,204}$	$T_{71,206}$	$T_{78,218}$	$T_{76,201}$	$T_{75,206}$	$T_{77,212}$	$T_{76,206}$	$T_{80,204}$	$T_{80,201}$	$T_{79,203}$

**Table 1.** Top 10 best mission locations compared between ISRU model and Joined model (J.) after t years in pixel area relation resized square tiles ( $T_{\phi \text{ index}, \lambda \text{ index}}$ ) with resolution  $\phi, \lambda$  of 15° (top), 5° (middle) and 1° (bottom). Indices starting at zero on  $(90^\circ \phi, -180^\circ \lambda)$  with  $-180^\circ$  to  $180^\circ$  Longitude range. Data from mass ratio  $r_m = 8.6$ .

298 top 10 of the ISRU ranking. The increased conservation of the highest ranked tiles can be explained  
299 by the coincidental overlap of low flight costs and low ISRU costs. In higher resolutions less tiles are  
300 shared, however due to the difference in percentage the top 10 make up for the whole set, the shared tiles  
301 are remaining substantial. Therefore, from Table 1 is concluded that the induced error during location  
302 selection is found to be small enough that a simplification, to only consider the ISRU effects, appears a  
303 valid approximation even for greater differences in  $\Delta v$  as in the analysed case.

## 4 DISCUSSION

304 The identification of the secondary relevance and even neglect of flight costs in the selected mission  
305 scenario can not directly be generalized without requirements, as for other ISRU production methods,  
306 target orbits, trajectories or mass ratios each of their influence can differ greatly from the analysed case.

307 However, under the given case of Ilmenite reduction and transport properties that are comparable or  
308 weaker than the analysed case, flight costs differences can be assumed insignificant. In particular, the  
309 major influence to verify in a quick assessment of a general case is the estimation of differences in  $\Delta v$   
310 requirements, which should be less than the analysed case of  $\approx 20\%$ . Lower mass ratios of the launcher  
311 are amplifying these differences in  $\Delta v$  when transferred to spent fuel and therefore fuel costs. Furthermore  
312 should be mentioned that this analysis featured a scenario which involved propellant refilling by own  
313 entities which reduces the fuel costs in general, which needs to be considered when other cost modelling is  
314 present. Additionally, the flight frequency is scaling up flight costs linearly and can compress the shift over  
315 time for the most optimal location, where as a rough reference value the delivered payload of 8 t per year  
316 can be considered from the analysed case.

317 Although a significant difference in the accessibility of the southern hemisphere was the result of the direct  
318 decent trajectory, it needs to be underlined that this does not conclude a worse accessibility from the NRHO  
319 to the southern hemisphere in general. In the chosen set of trajectories no options for intermediate parking

320 orbits are considered, which however if considered would bring these differences between northern and  
321 southern hemisphere down, as the 1 day transfer in May et al. (2020) shows entirely different characteristics.

322 As global lunar data is increasingly present, problems as these can be analysed and optimised close to  
323 their entirety over the whole lunar surface. Especially in the current stage of time where no infrastructure is  
324 yet deployed on the lunar surface, location selection can be carried by optimisation instead of dependencies  
325 by prior infrastructure.

326 To not create a prior infrastructure restriction ourselves, the plan for man-kinds presence and economics  
327 and even sustainability on the Moon should be expanded and seen in a bigger scope as much as possible.  
328 As this Oxygen propellant facility is just one entity of an economics network, which might move its most  
329 optimal location completely away in bigger context from its individually analysed location. Such a large  
330 scale technical investigation would make for a compelling future study.

## **CONFLICT OF INTEREST STATEMENT**

331 The authors declare hereby that the research was conducted in the absence of any commercial or financial  
332 relationships that could be construed as a potential conflict of interest.

## **AUTHOR CONTRIBUTIONS**

333 SS conducted the research, created the solution methods and wrote the paper. PZ did initiate the papers  
334 idea, supervised the research and reviewed the manuscript. DQ discussed orbital mechanics aspects and  
335 reviewed the manuscript.

## **FUNDING**

336 This research was conducted without any institutional funding. Publication fees are covered by the  
337 publication fund of the German Aerospace Center (DLR) in support for open access publishing.

## **DATA AVAILABILITY STATEMENT**

338 This work is providing open source on all processing steps performed in the corresponding Python  
339 Notebooks along with all resources in full resolution in the papers [Git-Repository](#).

## **REFERENCES**

- 340 [Dataset] David E. Smith (2015). 2009 lunar orbiter laser altimeter radiometry data set, lro-l-lola-3-radr-  
341 v1.0. doi:10.17189/1520639
- 342 [Dataset] Ernie Wright and Noah Petro (2019). SVS: CGI Moon Kit — svs.gsfc.nasa.gov. <https://svs.gsfc.nasa.gov/4720>. [Accessed 29-07-2023]
- 344 [Dataset] European Space Agency (2023). Argonaut - technical details. [https://www.esa.int/Science\\_Exploration/Human\\_and\\_Robotic\\_Exploration/Exploration/Argonaut](https://www.esa.int/Science_Exploration/Human_and_Robotic_Exploration/Exploration/Argonaut). [Accessed 08-09-2023]
- 347 Guerrero-Gonzalez, F. J. and Zabel, P. (2023). System analysis of an ISRU production plant: Extraction of  
348 metals and oxygen from lunar regolith. *Acta Astronautica* 203, 187–201. doi:10.1016/j.actaastro.2022.  
349 11.050

- 350 Kornuta, D., Abbud-Madrid, A., Atkinson, J., Barr, J., Barnhard, G., Bienhoff, D., et al. (2019). Commercial  
351 lunar propellant architecture: A collaborative study of lunar propellant production. *REACH* 13, 100026.  
352 doi:<https://doi.org/10.1016/j.reach.2019.100026>
- 353 Lee, D. E. (2019). White paper: Gateway destination orbit model: A continuous 15 year nrho reference  
354 trajectory (National Aeronautics and Space Administration (NASA)). Tech. Rep. Document ID:  
355 20190030294
- 356 May, Z. D., Qu, M., and Merrill, R. (2020). Enabling global lunar access for human landing systems  
357 staged at earth-moon l2 southern near rectilinear halo and butterfly orbits. In *AIAA Scitech 2020 Forum*  
358 (American Institute of Aeronautics and Astronautics). doi:10.2514/6.2020-0962
- 359 Nelson, D. M., Koeber, S. D., Daud, K., Robinson, M. S., Watters, T. R., Banks, M. E., et al. (2014).  
360 Mapping lunar maria extents and lobate scarps using lroc image products. *Lunar Planet. Sci.* 45, 2861
- 361 Papike, J. J., Simon, S. B., and Laul, J. C. (1982). The lunar regolith: Chemistry, mineralogy, and petrology.  
362 *Reviews of Geophysics* 20, 761–826. doi:<https://doi.org/10.1029/RG020i004p00761>
- 363 Perrin, T. M. and Casler, J. G. (2016). Architecture study for a fuel depot supplied from lunar resources. In  
364 *AIAA SPACE 2016* (American Institute of Aeronautics and Astronautics). doi:10.2514/6.2016-5306
- 365 Sargeant, H., Abernethy, F., Barber, S., Wright, I., Anand, M., Sheridan, S., et al. (2020). Hydrogen  
366 reduction of ilmenite: Towards an in situ resource utilization demonstration on the surface of the moon.  
367 *Planetary and Space Science* 180, 104751. doi:<https://doi.org/10.1016/j.pss.2019.104751>
- 368 Sato, H., Robinson, M. S., Lawrence, S. J., Denevi, B. W., Hapke, B., Jolliff, B. L., et al. (2017). Lunar  
369 mare tio 2 abundances estimated from uv/vis reflectance. *Icarus* 296, 216–238. doi:10.1016/j.icarus.  
370 2017.06.013
- 371 Trofimov, S., Shirobokov, M., Tselousova, A., and Ovchinnikov, M. (2020). Transfers from near-  
372 rectilinear halo orbits to low-perilune orbits and the moon's surface. *Acta Astronautica* 167, 260–271.  
373 doi:10.1016/j.actaastro.2019.10.049
- 374 Whitley, R., Davis, D., Burke, L., McCarthy, B., Power, R., McGuire, M., et al. (2018). Earth-moon near  
375 rectilinear halo and butterfly orbits for lunar surface exploration